Channel Modeling and Analysis for Wireless Networks in Underground Mines and Road Tunnels

Zhi Sun, *Student Member, IEEE,* and Ian F. Akyildiz, *Fellow, IEEE*

***Abstract*—Wireless networks can greatly facilitate the communication in underground mines and road/subway tunnels, where the propagation characteristics of electromagnetic (EM) waves are significantly different from those in terrestrial environments. According to the structure of underground mines and road tunnels, two types of channel models can be utilized, namely, tunnel and room/pillar channel models. However, there exists no theoretical model for room-and-pillar channel in underground mines to date, and current existing tunnel channel models do not provide an analytical solution for both near and far regions of the sources. In this paper, the multimode model is proposed, which provides an analytical expression for the received power and the power delay profile at any position in a tunnel. Moreover, the multimode model is extended to characterize the room-and-pillar channel in the underground mines after combining it with the shadow fading model. The theoretical models are validated by experimental measurements. Based on the proposed channel models, the effects of various factors on the signal propagation are analyzed. The factors include: the operating frequency, the size of the tunnel or underground mine room, the antenna position and polarization, and the electrical parameters.**

***Index Terms*—Wireless networks, underground mine, tunnel, channel model, waveguide, multi-mode model.**

I. Introduction

RELIABLE and efficient communication networks are needed in underground mines and road/subway tunnels. They can be used to improve the safety and productivity in underground mines [1], [2], to realize convenient communication for drivers and passengers in road/subway tunnels, and to avoid terroristic attacks by surveilling these vulnerable areas.

In underground mines and road tunnels, wireless networking using natural wave propagation is a more flexible and efficient solution than the wire-based or leaky coaxial cable guided systems because it is low-cost, easy to implement and scalable. However, radio waves do not propagate well in underground mines and road tunnels [5]. Due to the bounding of the tunnel walls, the propagation characteristics of electromagnetic (EM) signals are very different than in terrestrial wireless channels [4], [6]. To design an optimal wireless communication network in underground mines and road tunnels, an accurate channel model with realistic computational cost is needed to predict the path loss as well as the signal delay spread.

In underground mines, multiple passageways are developed to connect the aboveground entrance and different mining areas. The structure of mining area is established by mining methods, which are determined by the shape and position of the ore body [7].

- If the ore body is flat and competent, room and pillar mining can be implemented. The mining area can be viewed as a big room with some randomly shaped pillars in it, as shown in Fig. 1(a).
- If the ore body has a steep dip, cut-and-fill mining, sublevel stoping or shrinkage stoping can be employed. Mines using those techniques have similar structures: the mining area consists of several types of tunnels, e.g. mining tunnel and transport tunnel. The sectional plan of cut-and-fill mining is shown in Fig. 1(b).
- If the ore body has a large, thin, seam-type shape, longwall mining is preferred, as shown in Fig. 1(c). Besides the entry tunnels, the mining area near the longwall face can also be modeled as a tunnel since it is encircled by the hydraulic support and the longwall face.

Therefore, underground mines require two types of channel models. The *tunnel channel model* is used to describe the signal propagation in passageways and mining area tunnels. On the other hand, the *room-and-pillar channel model* characterizes the wireless channel of room-and-pillar mining areas. It should be noted that the structure of road/subway tunnels is similar to that of underground mine tunnels, thus they can share the same tunnel channel model.

For *room-and-pillar channel model*, no theoretical results have been obtained to date. For *tunnel channel model*, currently there are mainly three solutions [8]: the Geometrical Optical model (GO model), the Waveguide model and the Full Wave model. The GO model can numerically predict the path loss and signal delay at any position. However, it requires a large amount of information to describe the environment [9]. Additionally, for long tunnel paths, the very large number of rays leads to numerical difficulties and the convergence may become very long. The waveguide model does not need detailed information to describe the tunnel and it is the only model that provides the analytical solution. However, it is not suitable to analyze the signal propagation in the region near the transmitter. Consequently, it can not be utilized in high density networks, e.g., wireless sensor networks. The full wave model, such as finite-difference time-domain (FDTD) technique, provides very accurate results in arbitrary geometries. However, the model is limited to numerical results and also may create unrealistic computational burden.

In this paper, we provide an analytical channel model, the multimode model, which lays out the foundation for reliable and efficient communication networks in underground

Paper approved by K. K. Leung, the Editor for Wireless Network Access and Performance of the IEEE Communications Society. Manuscript received July 21, 2008; revised January 11, 2009, July 23, 2009, and November 23, 2009.

The authors are with the Broadband Wireless Networking Laboratory, School of Electrical & Computer Engineering, Georgia Institute of Technology, Atlanta, GA, 30332, USA. (e-mail: {zsun, ian}@ece.gatech.edu).

Digital Object Identifier 10.1109/TCOMM.2010.06.080353

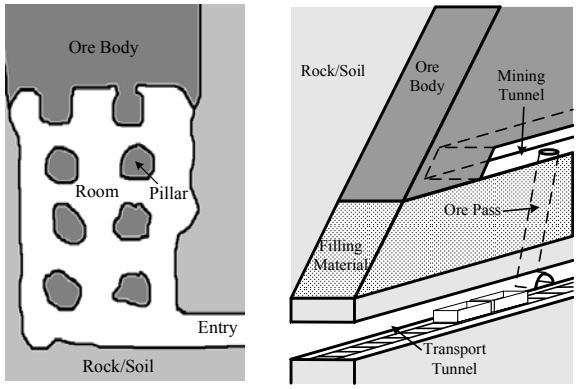

(a) Plan of room-and-pillar mining

(b) Cut-and-fill mining

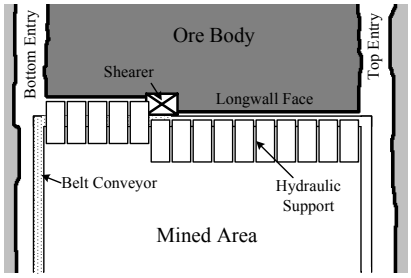

(c) Plan of longwall mining

Fig. 1. Mine structure of different mining methods.

mines and road tunnels. For tunnel environment, the multimode model can completely characterize the natural wave propagation in both near and far regions of the source. For room-and-pillar environment, the multimode model is still valid when combined with the shadow fading model. The proposed theoretical model is validated by the experimental measurements. Based on the new channel model, we present an in-depth analysis on the wireless channel characteristics in underground mines and road tunnels, which is influenced by multiple factors including operating frequency, tunnel or room size, antenna position and polarization, and dielectric properties of the wall/ceiling/floor, and the air in the mine or tunnel.

The remainder of this paper is organized as follows. In Section II, the related work is introduced. In Section III, the multimode model is developed in detail. Then, in Section IV, the characteristics of the wireless channel in underground mines and road tunnels is analyzed by the multimode model. Finally, the paper is concluded in Section V.

II. Related Work

Existing channel models for tunnels include the GO model [10], the waveguide model [11] and full wave model [12]. In the GO model, EM waves are approximately modeled as optical rays. The EM field is obtained by summing the contributions of rays undergoing reflections on the tunnel walls. In [13], [14], the rays diffracted near tunnel wedges are considered to improve the accuracy of the GO model. Except in some very idealized situations, e.g., the waveguide with two perfectly reflecting side walls [10], the GO model depends on computer simulations to obtain numerical solutions, and the computational burden increases dramatically as the signal path is prolonged [9], [15]. In the waveguide model, the tunnel behaves as an oversized waveguide with imperfectly lossy walls. Maxwell's equations are solved by taking consideration of the boundary conditions. The eigenfunctions and propagation constants for the EM field of all possible modes are provided in [16]. The waveguide model assumes that there is only the lowest mode signal propagation in the tunnel. However, since the operating frequency (UHF) is much higher than the cut-off frequency in tunnels, the large number of modes will be exited near the transmitter antenna [17]. Consequently, the waveguide model can not characterize the multi-mode operating channel in the near region. Full wave models can solve the Maxwell's equations with arbitrary boundary conditions using numerical methods, such as FDTD [12]. The partial differential equations are solved at discrete time and discrete points (finite grid). However, it is required that the size of the finite grid in space should be less than one tenth of the free space wavelength, and the time integration step must be less than the grid size divided by the velocity of the light. Given the large size of tunnels and the high operating frequency (UHF), the computational burden exceeds well beyond the capacity of existing computers.

In [18], a hybrid model combining the GO model and waveguide model is presented. A free-space model is utilized in the near region, and a waveguide model is used in the far region. The near and far regions are divided by the break-point (or turn-point), which is viewed as the intersection of the two different models. However, the change from near region with multiple modes to the far region with single mode is a continuous process. An exact break-point cannot exist. In addition, it cannot characterize the fast signal fluctuation of the multi-mode channel in the near region. Another type of hybrid model is the statistical model [19], [20], where the tunnel is divided into 2 or 3 intervals with different propagation coefficients. In each interval, the signal attenuation is roughly estimated by GO model or experimental results, and the signal fluctuation is modeled as Rayleigh and Rice distributions. Statistical model can simply predict both signal attenuation and fluctuation. However, the coefficients may be only applicable to a certain environment. Additionally, the model also encounters the problem of how to divide the intervals.

In [21], a mode-matching method is used to give a measure for the correlation of different antennas of a MIMO system in tunnels. The mode intensity is derived by projecting the field derived by GO model onto the orthogonal modes. However, this mode-matching method cannot provide the closed-form results of the mode intensity. Consequently, neither detailed analytical solution nor further analysis is given in [21].

Currently, there is no existing channel model for room-and-pillar mining area. In [4], [22], some experimental measurements are provided. It is indicated that the signal experiences higher attenuation in room-and-pillar environments than in tunnels. Additionally, the multipath fading is severe in both near and far region of the transmitter.

In this paper, we provide a new hybrid model that combines the GO model and waveguide model using Poisson sum formula. Analytical solutions for both near and far regions

are developed for tunnel environments. Combined with the shadow fading model, our model can also characterize the wireless channel in the room-and-pillar mining area. The proposed model is validated by both theoretical deduction and experimental results.

III. The Multimode Model

To settle the problems of current tunnel channel models, we introduce the multimode model, which can be viewed as a multi-mode operating waveguide model. Since the modes derived by the waveguide model are actually all possible solutions for the Maxwell's equations, only the EM waves that have the same shapes as those modes are possible to exist in the tunnel. However, the intensity of each mode depends on the excitation, which cannot be given by the waveguide model. Hence, the GO model is involved to analyze the EM field distribution for the excitation plane, i.e., the tunnel cross-section that contains the transmitter antenna. This field distribution can be viewed as the weighted sum of the field of all modes. The mode intensities are estimated by a mode-matching technique. Once the mode intensity is determined in the excitation plane, the mode propagation is mostly governed by the tunnel itself. Then the EM field in the rest of the tunnel can be predicted by summing the EM field of each mode.

The room-and-pillar environment can be viewed as a planar air waveguide superimposed with some random distributed and random shaped pillars in it. A simplified multimode model is able to describe the EM wave propagation in the planar air waveguide. The random distributed and random shaped pillars form an environment very similar to a terrestrial metropolitan area with many buildings. Hence, the shadow fading model can be used to describe the signal's slow fading caused by the reflection and diffraction on those pillars.

In the remainder of this section, we first develop the multimode model for tunnel channels. Then the multimode model is extended to cover the room-and-pillar case.

A. Tunnel Environment Model

Actual tunnel cross sections are generally in-between a rectangle and a circle. However, the EM field distribution and attenuation of the modes in rectangle waveguide are almost the same as the circular waveguide [4]. Hence, in our model, the tunnel cross section is treated as an equivalent rectangle with a width of $2a$ and a height of $2b$. A Cartesian coordinate system is set with its origin located at the center of the rectangle tunnel. k_v, k_h and k_a are the complex electrical parameters of the tunnel vertical/horizontal walls and the air in the tunnel, respectively, which are defined as: $k_v = \varepsilon_0\varepsilon_v + \frac{\sigma_v}{j2\pi f_0}$, $k_h = \varepsilon_0\varepsilon_h + \frac{\sigma_h}{j2\pi f_0}$ and $k_a = \varepsilon_0\varepsilon_a + \frac{\sigma_a}{j2\pi f_0}$, where ε_v, ε_h and ε_a are the relative permittivity for vertical/horizontal walls and the air in the tunnel; ε_0 is the permittivity in vacuum space; σ_v, σ_h and σ_a are their conductivity; f_0 is the central frequency of the signal. The three areas are assumed to have the same permeability μ_0. The wave number in the tunnel space is given by $k = 2\pi f_0\sqrt{\mu_0\varepsilon_0\varepsilon_a}$. We define the relative electrical parameter $\overline{k_v}$ and $\overline{k_h}$ for concise expression, which are $\overline{k_v} = k_v/k_a$ and $\overline{k_h} = k_h/k_a$. We assume that the transmitter antenna is an X-polarized electrical dipole. The results for Y-polarized antenna can be obtained simply by interchanging the x- and y-axes. The major polarized field plays a dominant role inside the tunnel and the coupling term can be omitted. Hence, in our multimode model, we only consider the major polarized field.

B. Multiple Mode Propagation in Tunnels

The propagation of EM waves in tunnels can be viewed as the superposition of multiple modes with different field distribution and attenuation coefficients. By solving the Maxwell's equations, the field distribution of each mode can be derived in the form of eigenfunctions [5], [16], [26]:

$$E^{eign}_{m,n}(x,y) \simeq \sin\Big(\frac{m\pi}{2a}x + \varphi_x\Big)\cdot\cos\Big(\frac{n\pi}{2b}y + \varphi_y\Big) \quad (1)$$

where $\varphi_x = 0$ if m is even; $\varphi_x = \frac{\pi}{2}$ if m is odd; $\varphi_y = 0$ if n is odd; $\varphi_y = \frac{\pi}{2}$ if n is even.

The field at any position (x, y, z) inside the tunnel can be obtained by summing up the field of all significant modes, which is given by:

$$E^{Rx}(x,y,z) = \sum_{m=1}^{\infty}\sum_{n=1}^{\infty} C_{mn}\cdot E^{eign}_{m,n}(x,y)\cdot e^{-(\alpha_{mn}+j\beta_{mn})\cdot z} \quad (2)$$

where C_{mn} is the mode intensity on the excitation plane; α_{mn} and β_{mn} are the attenuation coefficient and the phase-shift coefficient, respectively, which is given by [5], [11], [16]:

$$\alpha_{mn} = \frac{1}{a}\left(\frac{m\pi}{2ak}\right)^2 Re\frac{\overline{k_v}}{\sqrt{\overline{k_v}-1}} + \frac{1}{b}\left(\frac{n\pi}{2bk}\right)^2 Re\frac{1}{\sqrt{\overline{k_h}-1}}$$
$$\beta_{mn} = \sqrt{k^2 - \left(\frac{m\pi}{2a}\right)^2 - \left(\frac{n\pi}{2b}\right)^2} \quad (3)$$

The waveguide model considers that only the lowest order mode exists in the tunnel, i.e. $C_{11} = 1$ and $C_{mn} = 0$ if $(m,n) \neq (1,1)$. However, in the near region of the transmitter, there exist multiple modes. The intensity of each modes need to be determined. In the next step, we first analyze the field distribution of the excitation plane by the GO model. Then a mode matching technique is utilized to convert the sum of rays of the GO model to the sum of modes. Consequently, the mode intensity C_{mn} on the excitation plane can be obtained.

C. Field Analysis of the Excitation Plane by the GO Model

The total field in the tunnel is equal to the sum of ray contributions from all reflection images and the source. The reflection images and the source on the excitation plane are located as Fig. 2 shows. Due to the geometry characteristic of rectangle cross section shape, the images and the reflection rays have the following properties:

- The ray coming from image $I_{p,q}$ experiences $|p|$ times reflection from vertical wall and $|q|$ times reflection from horizontal ceiling/floor.
- Suppose that α is the incident angle on the ceiling/floor, and β is the incident angle on the wall. For a certain ray, these angles remain the same.

Consider that the transmitter is located at the coordinate $(x_0, y_0, 0)$, and the observation point is set at the coordinate (x, y, z). The field at the transmitter is E_0. The field at the

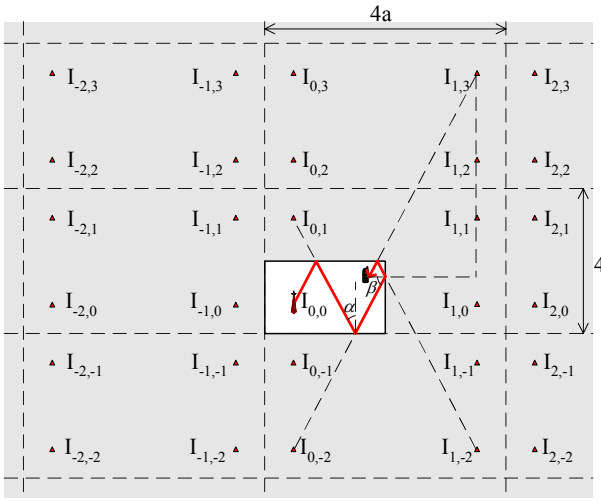

Fig. 2. The set of images in the excitation plane in a rectangular cross section tunnel.

observation point is the sum of the rays coming from all the images:

$$E^{Rx}(x,y,z) = E_0 \cdot \sum_{p=-\infty}^{\infty}\sum_{q=-\infty}^{\infty}\left[\frac{\exp(-jkr_{p,q})}{r_{p,q}}\right]\cdot S(\overline{k_v})^{|p|}\cdot R(\overline{k_h})^{|q|} \tag{4}$$

where $r_{p,q}$ is the distance between image $I_{p,q}$ and the receiver:

$$r_{p,q}=\sqrt{(2pa\pm x_0-x)^2+(2qb\pm y_0-y)^2+z^2}; \tag{5}$$

where "+" sign is for the case when p or q is even, while "−" sign is for that case when p or q is odd. $R(\overline{k_h})$ and $S(\overline{k_v})$ are the reflection coefficients on the horizontal and vertical walls. In this paper, the reflection coefficients $R(\overline{k_h})$ and $S(\overline{k_v})$ are simplified to their approximate expressions (see Appendix A):

$$R(\overline{k_h})=-\exp\left(\frac{-2}{\sqrt{\overline{k_h}-1}}\cdot\frac{|2qb\pm y_0-y|}{r_{p,q}}\right);$$
$$S(\overline{k_v})=-\exp\left(\frac{-2\overline{k_v}}{\sqrt{\overline{k_v}-1}}\cdot\frac{|2pa\pm x_0-x|}{r_{p,q}}\right) \tag{6}$$

D. Mode-Matching in the Excitation Plane

By rearranging the ray sum in (4), we can divide the ray sum into four parts:

$$\begin{aligned}E^{Rx}(x,y,z) &= \sum_{p,q=-\infty}^{\infty} f(4qa+x_0-x,4pb+y_0-y)\\ &+\sum_{p,q=-\infty}^{\infty} f(4qa+x_0-x,4pb+2b-y_0-y)\\ &+\sum_{p,q=-\infty}^{\infty} f(4qa+2a-x_0-x,4pb+y_0-y)\\ &+\sum_{p,q=-\infty}^{\infty} f(4qa+2a-x_0-x,4pb+2b-y_0-y)\end{aligned} \tag{7}$$

where $f(u,v)$ is the function defined as:

$$f(u,v)=E_0\frac{\exp(-jk\sqrt{u^2+v^2+z^2})}{\sqrt{u^2+v^2+z^2}}\cdot(-1)^{p(v)+q(u)} \cdot\exp\left[\frac{-2}{\sqrt{u^2+v^2+z^2}}\left(\frac{|v|p(v)}{\sqrt{\overline{k_h}-1}}+\frac{|u|\overline{k_v}q(u)}{\sqrt{\overline{k_v}-1}}\right)\right] \tag{8}$$

where $p(v)$ and $q(u)$ are discontinuous functions that takes values of $0,\pm1,\pm2,\cdots$. To facilitate the mode matching, we approximately transform $p(v)$ and $q(u)$ to continuous functions. Then,

$$p(v)=\frac{|v|}{2b};\quad q(u)=\frac{|u|}{2a} \tag{9}$$

Note that each part in (7) is a periodic function of $4a$ and $4b$. We first consider the first part in (7). According to 2-dimension Poisson Summation Formula [23], the sum can be converted to:

$$\begin{aligned}&\sum_{p,q=-\infty}^{\infty} f(4qa+x_0-x,4pb+y_0-y)\\ &\quad=\frac{1}{4a}\frac{1}{4b}\sum_{m=-\infty}^{\infty}\sum_{n=-\infty}^{\infty}\mathscr{F}_1(m,n)\cdot e^{j\frac{m\pi}{2a}x}e^{j\frac{n\pi}{2b}y}\end{aligned} \tag{10}$$

The coefficient $\mathscr{F}_1(m,n)$ is the 2-dimension Fourier transform of the function $f(x_0-x,y_0-y)$ in the first part in (7):

$$\mathscr{F}_1(m,n)=\iint_{-\infty}^{\infty} f(x_0-x,y_0-y)e^{-j\frac{m\pi}{2a}x}e^{-j\frac{n\pi}{2b}y}dxdy \tag{11}$$

We utilize the saddle-point method [24] to derive the closed-form result of the integration. The detailed deduction of the saddle-point integration are provided in Appendix B. Note that here we only care about the field $E^{Rx}(x,y,z)$ on the excitation plane where $z=0$. Therefore, the coefficient $\mathscr{F}_1(m,n)$ on the excitation can be expressed as:

$$\mathscr{F}_1(m,n)\simeq E_0\frac{\pi}{\sqrt{1-(\frac{m\pi}{2ak})^2-(\frac{n\pi}{2bk})^2}}\cdot e^{-j(\frac{m\pi}{2a}x_0+\frac{n\pi}{2b}y_0)} \tag{12}$$

By this way, the first part of the ray sum in (7) can be converted to the sum of complex modes in (10). In the same way, the Poisson sum formula can be utilized in the rest parts in (7), and the coefficients $\mathscr{F}_2(m,n),\mathscr{F}_3(m,n),\mathscr{F}_4(m,n)$ can also be derived by the saddle point method. Therefore, the field in the excitation plane can be expressed as:

$$\begin{aligned}E^{Rx}(x,y,0) &= \frac{1}{4a}\frac{1}{4b}\sum_{m=-\infty}^{\infty}\sum_{n=-\infty}^{\infty}\Big[\mathscr{F}_1(m,n)+\mathscr{F}_2(m,n)\\ &\quad+\mathscr{F}_3(m,n)+\mathscr{F}_4(m,n)\Big]\cdot e^{j\frac{m\pi}{2a}x}e^{j\frac{n\pi}{2b}y}\\ &=\sum_{m=-\infty}^{\infty}\sum_{n=-\infty}^{\infty}\frac{E_0\pi}{16ab\sqrt{1-(\frac{m\pi}{2ak})^2-(\frac{n\pi}{2bk})^2}}\cdot e^{j\frac{m\pi}{2a}x}e^{j\frac{n\pi}{2b}y}\\ &\quad\cdot\Big(e^{-j\frac{m\pi}{2a}x_0}e^{-j\frac{n\pi}{2b}y_0}+e^{j\frac{m\pi}{2a}x_0-m\pi}e^{j\frac{n\pi}{2b}y_0-n\pi}\\ &\quad-e^{j\frac{m\pi}{2a}x_0}e^{j\frac{n\pi}{2b}y_0-n\pi}-e^{j\frac{m\pi}{2a}x_0-m\pi}e^{j\frac{n\pi}{2b}y_0}\Big)\\ &=\sum_{m=1}^{\infty}\sum_{n=1}^{\infty}\frac{E_0\pi}{ab\sqrt{1-(\frac{m\pi}{2ak})^2-(\frac{n\pi}{2bk})^2}}\sin\Big(\frac{m\pi}{2a}x_0+\varphi_x\Big)\\ &\quad\cdot\cos\Big(\frac{n\pi}{2b}y_0+\varphi_y\Big)\sin\Big(\frac{m\pi}{2a}x+\varphi_x\Big)\cos\Big(\frac{n\pi}{2b}y+\varphi_y\Big)\end{aligned} \tag{13}$$

Note that (13) is exactly the weighted sum of the eigenfunction of each propagation mode in (1). The weight of each eigenfunction is the mode intensity C_{mn} in the excitation plane:

$$C_{mn} = \frac{E_0\pi}{ab\sqrt{1-(\frac{m\pi}{2ak})^2-(\frac{n\pi}{2bk})^2}}\sin\Big(\frac{m\pi}{2a}x_0+\varphi_x\Big)\cos\Big(\frac{n\pi}{2b}y_0+\varphi_y\Big) \tag{14}$$

By substituting (1), (3) and (14) into (2), the field of any position in the tunnel can be analytically calculated.

Then suppose the transmitting power is P_t; G_t and G_r are the antenna gains of the transmitter and the receiver, respectively. The predicted received signal power at the coordinate (x, y, z) is given by:

$$P_r(x,y,z) = P_tG_tG_r\left(\frac{1}{E_0}\sum_{m,n}C_{mn}\cdot E^{eign}_{m,n}(x,y)\cdot e^{-(\alpha_{mn}+j\beta_{mn})\cdot z}\right)^2 \tag{15}$$

E. Power Delay Profile for Wideband Signal

If the transmitting signal is wideband, significant signal distortion may happen due to the dispersion effect of the tunnel waveguide, which will cause severe inter symbol interference (ISI). We characterize this channel effect by calculating the power delay profile (PDP).

We assume that the wideband signal $s(t)$ has a bandwidth of B around the central frequency f_0, i.e. $f \in [f_0 - B/2, f_0 + B/2]$. The frequency spectrum of the signal is characterized by its fourier transform $S(f)$. This signal can be viewed as the sum of all the sinusoidal waves whose frequencies fall into the band. The intensity of each sinusoidal wave is determined by the fourier transform $S(f)$. In addition, if the signal $s(t)$ is real, then its fourier transform $S(f)$ is an even function of the frequency f. Hence,

$$s(t) = \int_{f_0-B/2}^{f_0+B/2} S(f)\cdot 2\cos(2\pi f\cdot t)\ df \tag{16}$$

Different frequency elements in (16) have different wave number $k(f)$. Consequently, the mode intensity $C_{mn}(f)$, field distribution $E^{eign}_{m,n}(x, y, f)$, attenuation coefficients $\alpha_{mn}(f)$ and phase-shift coefficients $\beta_{mn}(f)$ become the functions of the frequency f.

Moreover, the propagation delay of a certain mode also varies with the frequency. For a sinusoidal wave signal with a single frequency f, the propagation delay of EH_{mn} mode can be calculated by $\tau_{mn}(f) = z/v_{mn}(f)$, where $v_{mn}(f)$ is the group velocity that is given by:

$$v_{mn}(f) = c\sqrt{1-\left(\frac{c\sqrt{\left(\frac{m\pi}{2a}\right)^2+\left(\frac{n\pi}{2b}\right)^2}}{2\pi f}\right)^2} \tag{17}$$

According to (17), the group velocity is a function of both the operating frequency f and the mode's order (m, n). For the same mode, different frequency signals have different propagation delay. For a single frequency, different modes also have different delay. Hence, both the dispersion among modes and the dispersion among frequency elements should be considered when calculating the power delay profile of a wideband signal. At a certain time t and position (x, y, z) in the tunnel, the received power of a wideband signal P_{WB} can be calculated by summing up the contributions of all the arrived significant modes of all frequency elements, which is given by:

$$P_{WB}(x,y,z,t) = P_tG_tG_r\left\{\frac{1}{E_0}\sum_{m,n}\int_{f_0-\frac{B}{2}}^{f_0+\frac{B}{2}}\Big[C_{mn}(f)\cdot E^{eign}_{m,n}(x,y,f)\cdot e^{-\alpha_{mn}\cdot z}\cdot S(f)\cdot\delta(t-\frac{z}{v_{mn}(f)})\cdot\cos(2\pi ft-\beta_{mn}z)\Big]df\right\}^2 \tag{18}$$

where

$$\delta(x) = \begin{cases} 1, & \text{if } x \geq 0 \\ 0, & \text{otherwise} \end{cases} \tag{19}$$

Then the power delay profile can be derived by calculating (18) in a continuous time slot.

F. Multimode Model in the Room-and-pillar Environment

As discussed in the beginning of Section III, simplified multimode model combined with shadow fading model is implemented to characterize the wireless channel in room-and-pillar environment.

1) The Simplified Multimode Model: Because the room of the room-and-pillar channel in underground mines is usually very large, the influence of the reflection on the vertical walls is very limited. However, the reflection on the ceiling and floor cannot be omitted. Hence, the room without pillars is modeled as a planar air waveguide. It can be viewed as a simplified rectangular waveguide with dependence on only one coordinate. Hence, we use the same procedure as in the tunnel case to develop the multimode model in room-and-pillar environment.

First, we utilize the GO model to analyze the excitation area. Because the planar air waveguide has dependence on only one coordinate, the excitation plane is degenerated to a line that is perpendicular to the ceiling and floor plane and contains the point of the transmission antenna. The geometry of the cross section is just the same as that of tunnels but with only y-coordinate. The properties of the images and the reflection rays in the tunnel case is still valid. The difference lies in: 1) only y-coordinate takes effect; and 2) the incident angle on the ceiling and floor is a constant – 0°, hence the reflection coefficient is $(1-\sqrt{k_h})/(1+\sqrt{k_h})$ for X-polarized field and $(\sqrt{k_h}-1)/(\sqrt{k_h}+1)$ for Y-polarized field. In the following derivation, we assume the transmission antenna is X-polarized. The result for Y-polarized antenna can be derived in the similar way. Consider that the transmitter is located at the height y_0, and the observation point is set at the height y. The major field at the observation point is given by:

$$E^{Rx} = E_0\cdot\sum_q\left[\frac{\exp(-jky_q(y))}{y_q(y)}\right]\cdot\left(\frac{1-\sqrt{k_h}}{1+\sqrt{k_h}}\right)^{|q|} \tag{20}$$

where $y_q(y)$ is the distance between image I_q and the receiver, which is given by:

$$y_q(y) = \begin{cases} |2qb-y_0-y|, & \text{if } q \text{ is odd} \\ |2qb+y_0-y|, & \text{if } q \text{ is even} \end{cases} \tag{21}$$

Second, we express the field on the excitation line obtained above into the weighted sum of planar air waveguide modes, and then derive the mode intensity. The eigenfunctions of X-polarized modes in planar air waveguide is given by [9]:

$$E_n^x(y) = E_0 \cdot \cos\left[\left(\frac{n\pi}{2b} - j \cdot \frac{n\pi}{2b^2 k}\frac{k_h}{\sqrt{k_h - 1}}\right) y + \varphi_y\right] \simeq E_0 \cdot \cos\left(\frac{n\pi}{2b} y + \varphi_y\right) \quad (22)$$

where $\varphi_y = \frac{\pi}{2}$ if n is even; $\varphi_y = 0$ if n is odd.

The mode intensity C_n is derived by converting the ray sum in (20) into mode sum using the Poisson sum formula. By using the same saddle point method as in the tunnel case, the mode intensity C_n is:

$$C_n(z) = \frac{E_0 \pi}{bz\sqrt{1 - (\frac{n\pi}{2bk})^2}} \cdot \cos\left(\frac{n\pi}{2b} y_0 + \varphi_y\right) \quad (23)$$

Note the intensity C_n is now a function of the distance z. With the intensity and eigenfunction of each mode, the field at any position can be predicted for the case without pillars.

2) Shadow Fading Model and the Combined Result: The pillars in the room-and-pillar mining area are randomly distributed and have random shapes. Signals may experience many reflection and diffraction on those pillars before reaching the receiver. It is very similar to the terrestrial metropolitan area with many buildings. Hence, the shadow fading model can be used to describe the signal's slow fading caused by the reflection and diffraction on those pillars. The amplitude change caused by shadow fading is often modeled using a log-normal distribution [25]. Since one mode can be viewed as a cluster of rays with the same grasping angle, we assume that each mode experiences identically distributed and independent shadow fading when it goes through the pillars. Therefore, the predicted field at any position ($b + y$ m above the floor, z m apart the transmitter) can be obtained by summing up the field of all modes, which is given by:

$$E^{Rx}(y, z) = E_0 \cdot \sum_n C_n(z) \cdot E_n^x(y) \cdot e^{-(\alpha_n + j\beta_n)\cdot z} \cdot \chi_n \quad (24)$$

where $\{\chi_n\}$ are identically distributed and independent log-normal random variables; the field is divided by $2\pi z$ because the plane wave in the room-and-pillar environment spreads in all horizontal directions; α_n is the attenuation coefficient and β_n is the phase-shift coefficient, which is given by [5], [9]:

$$\alpha_n = \frac{1}{b}\left(\frac{n\pi}{2bk}\right)^2 Re\frac{1}{\sqrt{k_h - 1}}; \quad \beta_n = \sqrt{k^2 - \left(\frac{n\pi}{2b}\right)^2} \quad (25)$$

In the room-and-pillar environment, since the shape, number and position of the pillars are random and vary from case to case, it is not possible to derive a general analytical solution to calculate the power delay profile. Consequently, to characterize the signal distortion of wideband signals in the room-and-pillar environments, field experiments are needed to measure the power delay profile in such mining areas.

G. Comparison with Experimental Measurements

To validate the multimode model, we compare our theoretically predicted received power with the experimental measurements in both tunnel and room-and-pillar environments provided in [3] and [4]. Additionally, we also compare our calculated power delay profile with the experimental measurements in a tunnel shown in [13].

In [3], the experiments were conducted in a concrete road tunnel. The tunnel is 3.5 km long and has an equivalent rectangle (7.8 m wide and 5.3 m high) cross section shape. The transmitting and receiving antennas are vertical polarized dipoles at the same height (2 m). Both antennas are placed at the same horizontal position of one-quarter of the tunnel width. Using the same parameters stated above, we calculated the received power by the multimode model. In Fig. 3(a), the calculated results at the frequency of 450 MHz and 900 MHz are compared with the measurements shown in [3, Fig. 18]. The theoretical curves are vertically displaced from the experimental curves for better comparison. It is shown that the curves of the theoretical and experimental results are close to each other. Our multimode model accurately predicts the attenuation velocity, the fast fading in the near region, the flat fading in the far region and the effects of different operating frequency in the tunnel environment.

In [4], the experiments were conducted in a room-and-pillar mining area with an average height of 6 m. The ceiling and floor are made of rocks and the typical values of electrical parameters are $\varepsilon_h = 10\varepsilon_0$ and $\sigma_h = 0.01$ S/m. The air in this mining area has the same electrical parameters as the atmosphere. The transmitting and receiving antennas are vertical polarized dipoles placed at the same height (2 m). In Fig. 3(b), the calculated results in the frequency of 900 MHz are compared with the measurements shown in [4, Fig. 8 (b)]. As it can be seen, the theoretical results have a good agreement with the experimental measurements in the room-and-pillar environment in underground mines.

In [13], wide-band propagation measurements were performed in a rectangular concrete subway tunnel that is 3.43 m wide, 2.6 m high and 258.7 m long. The signal has a 400 MHz bandwidth at the central frequencies of 900 MHz. The noise floor is 84 dBm, which yields a threshold of 74 dBm for an input 10 dB SNR. The transceiver antennas are horizontally polarized at the center of the tunnel and 50 m apart. In our estimation, we use 900 MHz carrier to modulate a 10 ns wide raised-cosine pulse, which has the same signal bandwidth and central frequency as the experiments. In Fig. 3(c), the calculated power delay profile is compared with the measurements shown in [13, Fig. 8 (a)]. It indicates that the theoretical results have a good match with the measurements in signal shape, delay spread and signal strength.

IV. Channel Characteristics in Underground Mines and Road Tunnels

In this section, we first implement the multimode model to analyze the path loss and delay spread under various tunnel conditions. Then we extend our analysis on path loss to the room-and-pillar case.

A. The Tunnel Environment

Except studying the effects of certain parameters, the default values are set as follows: The tunnel cross section shape is a rectangle with a height of 6 m and a width of 10 m; the

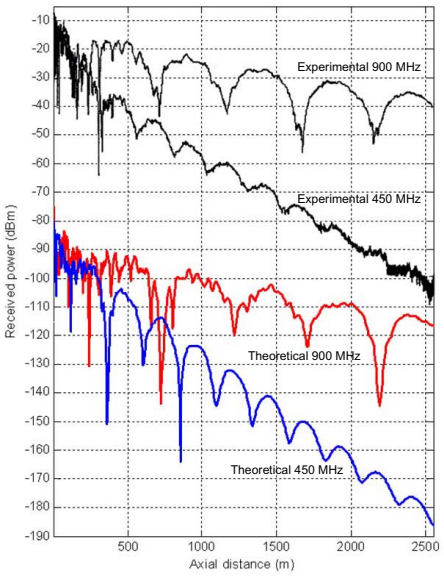

(a) Received power of 450 MHz and 900 MHz signals in a road tunnel (the theoretical result is displaced 75 dB downward).

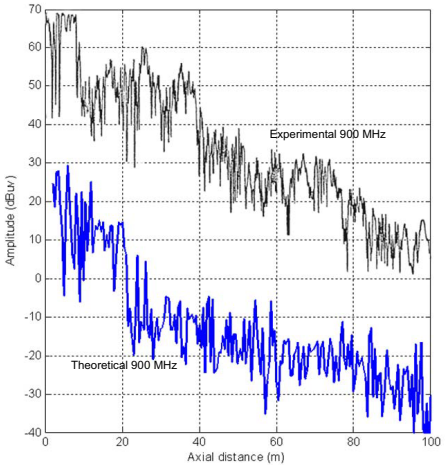

(b) Received power of 900MHz signal in a room-and-pillar mining area (the theoretical one is displaced 40 dB downward).

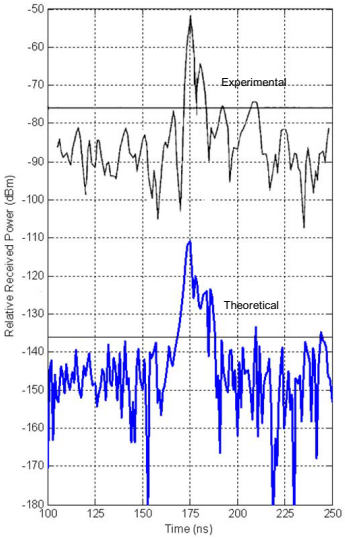

(c) Power delay profile in a Tunnel. The signal bandwidth is 400 MHz and the central frequency is 900 MHz. Transceivers are 50 m apart. The theoretical result is displaced 60 dB downward.

Fig. 3. Experimental and theoretical received power.

tunnel wall, ceiling and floor are made of the same material with electrical parameters $\varepsilon = 5\varepsilon_0$, $\sigma = 0.01\ S/m$; the tunnel interior is filled with air ($\varepsilon = \varepsilon_0$, $\sigma = 0\ S/m$). The operating frequency (carrier frequency) is set to 1 GHz. The wideband signal is a 20 ns wide raised-cosine pulse, which has a bandwidth of 200 MHz. The noise floor for the wideband signal is set to 90 dBm according to the strategy in [13]. It yields a threshold of 80 dBm for an input 10 dB SNR. The transmitting power is assumed to be 0 dBm. The transmitting and receiving antennas are horizontal polarized dipoles at the same height (one-third of the tunnel height). Both antennas are placed at the same horizontal position of one-quarter of the tunnel width.

1) The Operating Frequency: In Fig. 4 we illustrate the effects of operating frequency on the path loss in tunnels. Specifically, in Fig. 4(a) and Fig. 4(b) we give the signal power and the corresponding power distribution among significant modes as a function of axial distance at the frequency of 500 MHz and 1.0 GHz. The curve of the signal power can be divided into two regions. In the near region, the power attenuates fast and fluctuates very rapidly. This is attributed to the combined effect of multiple modes. While in the far region, the fall in the signal power is gradual. This is due to the fact that the higher order modes attenuate very fast as the distance increases. Hence, the field in the far region is governed by the few low-order modes left. The relationship between power distribution among modes and the received power is clearly shown in Fig. 4(a) and Fig. 4(b). Although the operation frequency does not affect the power distribution of modes significantly, it has an obvious influence on the propagation constants. Signals with higher frequency attenuate slower. Thus, as the frequency increases, the signal attenuation decreases and the fast fluctuating region is prolonged, as shown in Fig. 4(b).

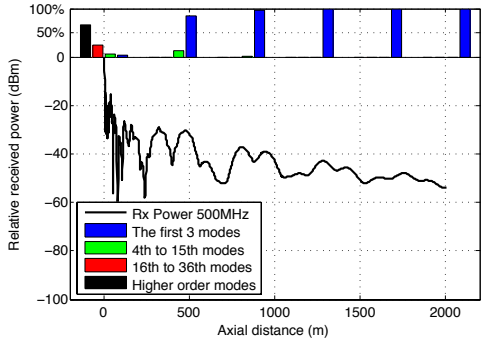

(a) Received signal power and the power distribution among modes at 500 MHz.

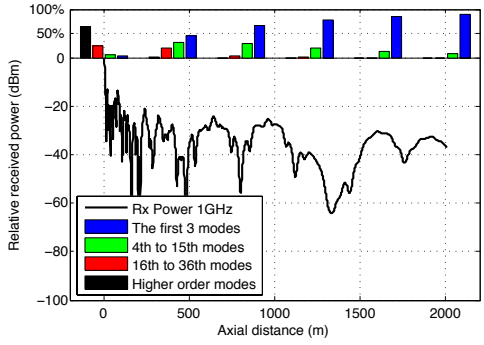

(b) Received signal power and the power distribution among modes at 1 GHz.

Fig. 4. Received power in tunnels at different operating frequencies.

In Fig. 5 we analyze the effect of operating frequency and transmission distance on the power delay profile in tunnels. It is shown that the raised-cosine pulse is widened and the pulse shape is distorted after propagation in the tunnel, which is caused by the following two reasons: 1) each frequency

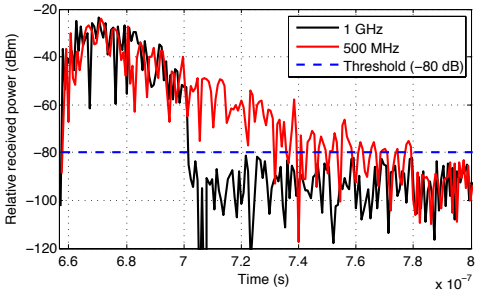

(a) Power delay profile at 200 m.

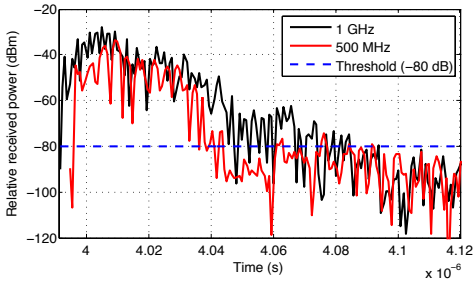

(b) Power delay profile at 1200 m.

Fig. 5. Power delay profile in tunnels at different operating frequencies.

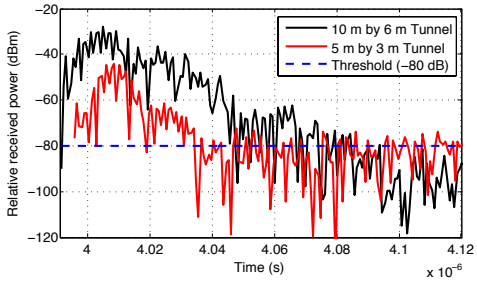

Fig. 6. Power delay profile in tunnels with different tunnel sizes at 1200 m.

element and the each mode of the original signal has different propagation delay; and 2) the attenuation and phase-shift rates of different frequency elements and modes are also different. As shown in Fig. 5(a), the delay spreads of the 500 MHz signal is larger than that of the 1 GHz signal when the transmission distance is 200 m. This is because that: 1) there are multiple significant modes for both frequency in the near region; 2) for the signal with lower operating frequency, the differences of group velocity between the frequency elements are larger, which causes larger delay spread. As the transmission distance increases to 1200 m, only lower order modes of the 500 MHz signal are left due to its high attenuation rate. Meanwhile the 1 GHz signal still has several significant modes at 1200 m. Hence the delay spread of the 1 GHz signal is larger in the far region. For the same signal with different transmission distance, it is observed that the delay spread increases as the distance increases, which is because that the difference of propagation delays among the modes and frequency elements increases as the transmission distance increases. However, after a certain distance, as higher order modes disappear in the far region, fewer modes are left and the delay spread decreases. Therefore, the delay spread is a function of distance, which is an increasing function at first and become a decreasing function after a turning point.

2) The Tunnel Size: The tunnel size has similar effects on the path loss and the delay spread as the operating frequency. In larger dimension tunnels, the attenuation constant $\left(\alpha_{mn}\right.$ in eq (3)$\left.\right)$ is smaller. Thus, more mode remains significant in far regions. Therefore, the speed of the signal attenuation decreases and the fast fluctuating region is prolonged in the larger tunnels. Moreover, since there are more significant modes in the larger dimension tunnel, the delay spread of the signal in such tunnel is also larger, as shown in Fig. 6. For horizontal polarized antennas, the tunnel width plays a more important role because the reflection coefficients on the horizontal ceiling and floor are larger than those on the vertical walls. Similarly, the tunnel height weights more for vertical polarized antenna.

3) The Antenna Position and Polarization: As discussed above, the mode attenuation is mostly determined by the tunnel size and operating frequency. The mode intensity is to a large extent governed by the position of the transmitter antenna. In Fig. 7 we give the received power and power distribution among modes with different antenna positions and polarizations. In Fig. 7(a) we show the case that the transmitter antenna is placed near the center of the tunnel cross section. The receiver antenna is placed either at the center or at the marginal position that is one-eighth of the tunnel height and one-eighth of the width. It is shown that the lowest modes are effectively excited. If the receiver is also at the center, both the signal attenuation and the fluctuation are small. If the receiver is placed near the tunnel walls, the attenuation and fluctuation are much more significant. In Fig. 7(b) we show the case that the transmitter antenna is placed near the tunnel wall ($1/8$ of the width and $1/8$ of the height). The receiver antenna is also placed either at the center or at the margin of the tunnel. Near the excitation plane, the high order modes play the dominant role. In this case, the position of receiver antenna does not affect the received signal as much as the former case. The attenuation and fluctuation of received power is significant, no matter where the receiver is placed.

Besides the antenna position, we analyze different antenna polarization in Fig 7(c). To make the effects more obvious, we choose a wide but low tunnel ($10 \times 3\ m^2$) here. We show that the signal excited from a horizontal polarized antenna attenuates much slower than that excited from a vertical polarized one. It is consistent with the previous discussion about the relationship between the tunnel size and antenna polarization. Hence, it can be pointed out that: in wide but low tunnel, the horizontal polarized antenna is more appropriate while for narrow but high tunnel, the vertical polarized antenna is more suitable.

In Fig. 8, we investigate the effect of antenna position and polarization on the power delay profile in tunnels. In particular, we show the case that the transmitter antenna is placed near the center of the tunnel cross section in Fig. 8(a). The case that the transmitter antenna is placed near the tunnel wall is shown in Fig. 8(b). The comparison between the power delay profiles of different polarizations is given in Fig. 8(c). It is shown that the delay spread is determined by the power of existing modes and the noise level. If more modes have much higher

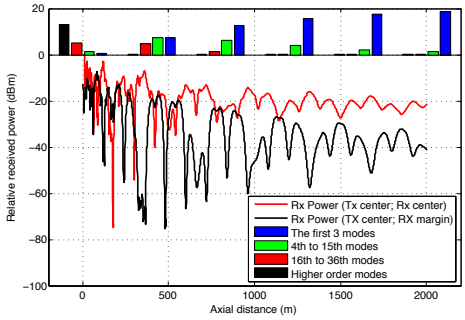

(a) Received signal power and the power distribution among modes when Tx antenna is placed near the tunnel center.

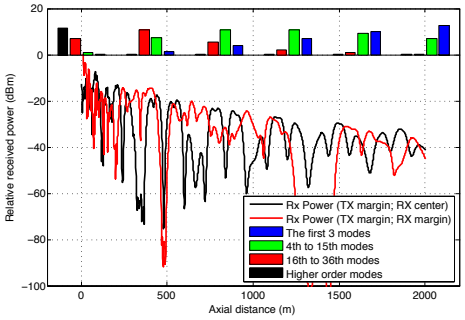

(b) Received signal power and the power distribution among modes when Tx antenna is placed near the tunnel wall.

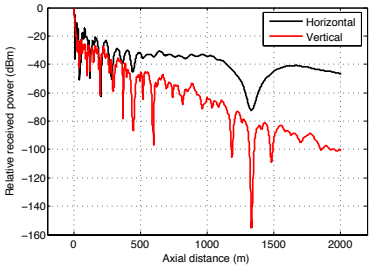

(c) Received signal power of different antenna polarization.

Fig. 7. Path loss characteristics in tunnels with different antenna position and polarization.

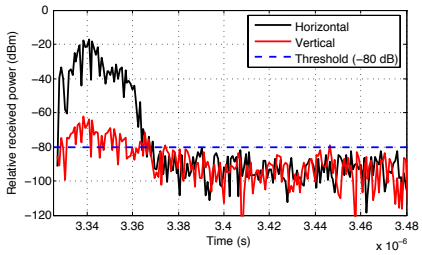

(a) Power delay profile when Tx antenna is placed near the tunnel center.

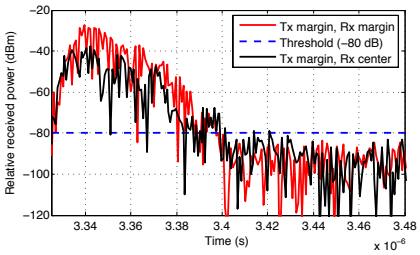

(b) Power delay profile when Tx antenna is placed near the tunnel wall.

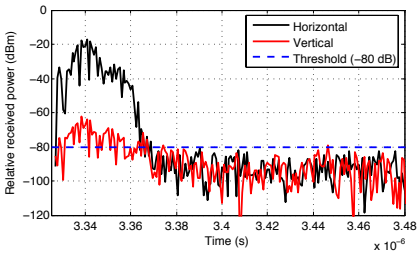

(c) Power delay profile of different antenna polarization.

Fig. 8. Power delay profile in tunnels with different antenna position and polarization at 1000 m.

power level than the noise, the delay spread is relatively larger. Otherwise, although the pulse is widened, most of the pulse is submerged in the noise and only a small portion of the pulse can be observed. Hence, for different antenna positions, the delay spread of the case when both transceivers are placed in the tunnel center is much larger than other cases. For different antenna polarizations, the delay spread of horizontal polarized antenna is larger than the vertical polarized one in wide tunnels where the width is larger than the height.

4) The Electrical Parameters: The electrical parameters consist of permittivity ε and conductivity σ. The temperature, humidity and pressure have little influence on the air permittivity but may affect the conductivity more. However, the effect of different conductivity of tunnel air may be neglectable, because it is very small compared to the permittivity. Therefore, the electrical parameters of tunnel air can be considered the same as those of atmosphere air. Tunnel walls' electrical parameters can be looked up in [5], where the permittivity of tunnel materials are in the range of $5\varepsilon_0 \sim 10\varepsilon_0$ and the conductivity is on the order of 10^{-2} S/m at the UHF frequency band. In this value range, the received power curves with different wall electrical parameters are very close to each other. Hence it can be concluded that the electrical parameters of either tunnel wall or tunnel air do not considerably influence the signal propagation inside the tunnel.

B. The Room-and-Pillar Environment

We conduct similar simulations in the room-and-pillar environment under the condition that: 1) the average height of the room is 6 m; 2) the electrical parameters of the ceiling and floor are $\varepsilon_h = 7\varepsilon_0$ and $\sigma_h = 0.01$ S/m; 3) the air in this mining area has the same electrical parameters as the atmosphere ($\varepsilon_a = \varepsilon_0$ and $\sigma_h = 0$ S/m); and 4) the transmitting and receiving antennas are vertical polarized dipoles placed at the same height (2 m). The transmitting power is assumed to be 0 dBm.

We give the received power in dB and the corresponding power distribution among significant modes as a function of axial distance at the frequency of 500 MHz and 1.0 GHz in Fig. 9(a) and Fig. 9(b), respectively. It can be observed that the signal attenuates faster in the near region of the source than in the far region. Due to the shadow fading and multiple-mode operating, signals experience significant fluctuations in both near and far region. Since higher frequency signal has lower attenuation coefficients, more number of modes remain significant in the far region. However, due to the shadow fading caused by the pillars and the path loss caused by the plane wave spreading, signal propagation with different operating frequency does not have significant differences.

Besides the operating frequency, other factors such as room height, antenna position/polarization and electrical parameters in the room-and-pillar environment affect signal propagation in a similar way as in the tunnel case. However, their influence is much smaller, which can be explained as follows. Compared to the tunnel case, signals in the room-and-pillar mining area experience extra multipath fading caused by the pillars. Moreover, higher path loss is experienced by the wave spreading in the room.

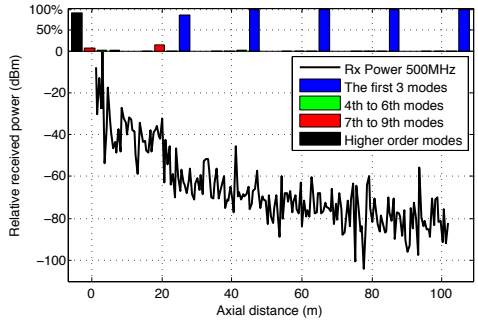

(a) Received signal power and the power distribution among modes at 500 MHz.

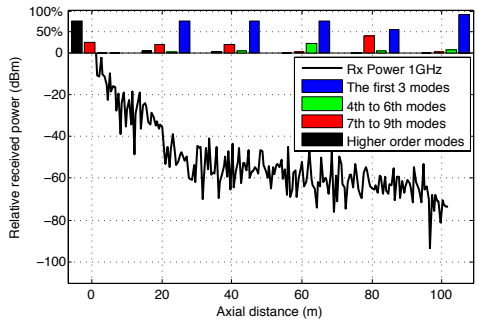

(b) Received signal power and the power distribution among modes at 1 GHz.

Fig. 9. Path loss characteristics in room-and-pillar environments with different operating frequencies.

V. Conclusion

Accurate and applicable channel model is needed to predict the wireless propagation characteristics in underground mines and road tunnels. We analyze the typical structures of current underground mines and road tunnels, and divide the channels in those environments into two cases: tunnel channel and room-and-pillar channel. Currently there is no theoretical channel model for the room-and-pillar case. Existing tunnel channel models do not provide an analytical solution for both near and far regions. In this paper, we develop the multimode model to address those problems. Based on the proposed channel model, our analysis shows that:

- For tunnel environment:
  1) Due to the combination of multiple modes, high signal attenuation and intense fluctuation occur in the near region. The fall in the received power is gradual in the far region because the higher order modes attenuate very fast as the distance increases. The division of near and far region depends on the operation frequency, the tunnel size and the transmitter positions, which is quantitatively analyzed for the first time.
  2) The attenuation is mostly determined by the tunnel size and operating frequency, while the power distribution among modes is governed by the position of the transmitter's antenna.
  3) The delay spread of the wideband signals is determined by how many significant modes exist and how long the transmission distance is.
  4) The humidity, pressure and temperature of the tunnel air, as well as the material of tunnel walls have little influence on the signal propagation in tunnels.
- For room-and-pillar environment:
  Signal propagation has similar characteristics as in the tunnel case. The difference is that signals experience significant fluctuations in both near and far regions. Additionally, the operating frequency, the room height, the antenna position/polarization and the electrical parameters have much smaller influence on the channel characteristics in the room-and-pillar environment than in the tunnels.

Appendix A
Simplification of Reflection Coefficients

If the tunnel size is much larger than the free-space wavelength of the incidence wave, the reflection coefficients are given by [27]:

$$R(\overline{k_h}) = \frac{\cos\alpha - \sqrt{\overline{k_h} - \sin^2\alpha}}{\cos\alpha + \sqrt{\overline{k_h} - \sin^2\alpha}};$$
$$S(\overline{k_v}) = \frac{\overline{k_v}\cos\beta - \sqrt{\overline{k_v} - \sin^2\beta}}{\overline{k_v}\cos\beta + \sqrt{\overline{k_v} - \sin^2\beta}} \quad \text{(A.1)}$$

where α is the incident angle of rays on the horizontal ceiling/floor; and β is the incident angle of rays on the vertical walls. Since we only consider the rays with small grazing angle (otherwise the path loss is huge), $R(\overline{k_h})$ and $S(\overline{k_v})$ can be approximated as:

$$R(\overline{k_h}) = -\exp\left(\frac{-2\sin\alpha}{\sqrt{\overline{k_h}-1}}\right);\ S(\overline{k_v}) = -\exp\left(\frac{-2\overline{k_v}\sin\beta}{\sqrt{\overline{k_v}-1}}\right) \quad \text{(A.2)}$$

Appendix B
Saddle Point Method

2-dimensional saddle point method [24] provides the approximate integration results of the form $\int_a^b\int_c^d g(u,v)e^{h(u,v)}dudv$. The integration in (11) has exactly the same form, where

$$g(u,v) = \frac{E_0}{\sqrt{u^2+v^2+z^2}} \quad \text{(B.1)}$$

$$h(u,v) = -jk\sqrt{u^2+v^2+z^2} - j\frac{m\pi}{2a}(x_0-u) \quad \text{(B.2)}$$
$$- j\frac{n\pi}{2b}(y_0-v) - \frac{2}{\sqrt{u^2+v^2+z^2}}\left(\frac{|v|p(v)}{\sqrt{\overline{k_h}-1}} + \frac{|u|\overline{k_v}q(u)}{\sqrt{\overline{k_v}-1}}\right)$$

Note that the last term in (B.2) can be omitted since $\sqrt{u^2+v^2+z^2}$ is much larger than 1.

The saddle point of the integration is (u_0, v_0) so that $\frac{\partial h(u,v)}{\partial u}|_{u=u_0} = 0$ and $\frac{\partial h(u,v)}{\partial v}|_{v=v_0} = 0$. Hence the saddle point for (11) can be calculated as:

$$u_0 = |z|\cdot\tan\theta_m; \qquad v_0 = |z|\cdot\tan\theta_n \quad \text{(B.3)}$$

where

$$\theta_m = \arcsin\frac{m\pi}{2ka}; \qquad \theta_n = \arcsin\frac{n\pi}{2kb} \quad \text{(B.4)}$$

Then the approximate results of the integration can be expressed as:

$$\iint_{-\infty}^{\infty} g(u,v)e^{h(u,v)}dudv \simeq \quad \text{(B.5)}$$
$$g(u_0,v_0)\cdot e^{h(u_0,v_0)}\cdot\frac{\pi}{\sqrt{\left|\frac{\partial^2 h(u_0,v_0)}{\partial u^2}\right|\cdot\left|\frac{\partial^2 h(u_0,v_0)}{\partial v^2}\right| - \left(\frac{\partial^2 h(u_0,v_0)}{\partial u\partial v}\right)^2}}$$

By this way, the approximate result of the integration in (11) can be obtained by substituting (B.1), (B.2) and (B.3) into (B.5), and finally we derive the closed-form expression shown in (12).

ACKNOWLEDGMENT

This work is based upon work supported by the US National Science Foundation (NSF) under Grant No. CCF-0728889.

REFERENCES

[1] I. F. Akyildiz and E. P. Stuntebeck, "Wireless underground sensor networks: research challenges," *Ad Hoc Netw. J. (Elsevier)*, vol. 4, pp. 669-686, July 2006.

[2] A. Chehri, P. Fortier, and P. M. Tardif, "Security monitoring using wireless sensor networks," in *Proc. Commun. Netw. Services Research (CNSR'07)*, pp. 13-17, May 2007.

[3] D. G. Dudley, M. Lienard, S. F. Mahmoud, and P. Degauque, "Wireless propagation in tunnels," *IEEE Antenna Propag. Mag.*, vol. 49, no. 2, pp. 11-26, Apr. 2007.

[4] M. Lienard and P. Degauque, "Natural wave propagation in mine environments," *IEEE Trans. Antenna Propag.*, vol. 48, no. 9, pp. 1326-1339, Sep. 2000.

[5] P. Delogne, *Leaky Feeders and Subsurface Radio Communications*. New York: Stevenage, Herts; P. Peregrinus, Aug. 1982

[6] P. Mariage, M. Lienard, and P. Degauque, "Theoretical and experimental approach of the propagation of high frequency waves in road tunnels," *IEEE Trans. Antenna Propag.*, vol. 42, no. 1, pp. 75-81, Jan. 1994.

[7] R. E. Gertsch and R. L. Bullock, *Techniques in Underground Mining: Selections from Underground Mining Methods Handbook*. Littleton, CO: Society for Mining, Metallurgy, and Exploration, 1998

[8] C. Cerasoli, "RF propagation in tunnel environments," in *Proc. IEEE Military Commun. Conf. (MILCOM'04)*, vol. 1, pp. 363-369, Nov. 2004.

[9] D. Porrat, "Radio propagation in hallways and streets for UHF communications," Ph.D. thesis, Stanford University, 2002.

[10] S. F. Mahmoud and J. R. Wait, "Geometrical optical approach for electromagnetic wave propagation in rectangular mine tunnels," *Radio Science*, vol. 9, no. 12, pp. 1147-1158, Dec. 1974.

[11] A. G. Emslie, R. L. Lagace, and P. F. Strong, "Theory of the propagation of UHF radio waves in coal mine tunnels," *IEEE Trans. Antenna Propag.*, vol. AP-23, no. 2, pp. 192-205, Mar. 1975.

[12] A. Taflove and S. C. Hagness, *Computational Electrodynamics: The Finite-Difference Time-Domain Method*, 3rd edition. Norwood, MA: Artech House, 2005.

[13] Y. Hwang, Y. P. Zhang, and R. G. Kouyoumjian, "Ray-optical prediction of radio-wave propagation characteristics in tunnel environments: theory, analysis and measurements," *IEEE Trans. Antenna Propag.*, vol. 46, no. 9, pp. 1328-1345, Sep. 1998.

[14] Y. P. Zhang and H. J. Hong, "Ray-optical modeling of simulcast radio propagation channels in tunnels," *IEEE Trans. Veh. Technol.*, vol. 53, no. 6, pp. 1800-1808, Nov. 2004

[15] S. Zhang, "The multipath propagation model of rectangular tunnel channel," in *Proc. IEEE TENCON 2002*, vol. 2, pp. 1016-1019, Oct. 2002.

[16] K. D. Laakmann and W. H. Steier, "Waveguides: characteristic modes of hollow rectangular dielectric waveguides," *Appl. Optics*, vol. 15, no. 5, pp. 1334-1340, May 1976.

[17] Y. P. Zhang, G. X. Zheng, and J. H. Sheng, "Excitation of UHF radio waves in tunnels," *Microwave Optical Technol. Lett.*, vol. 22, no. 6, pp. 408-410, Aug. 1999.

[18] Y. P. Zhang, "Novel model for propagation loss prediction in tunnels," *IEEE Trans. Veh. Technol.*, vol. 52, no. 5, pp. 1308-1314, Sep. 2003.

[19] M. Lienard and P. Degauque, "Propagation in wide tunnels at 2 GHz: a statistical analysis," *IEEE Trans. Veh. Technol.*, vol. 47, no. 4, pp. 1322-1328, Nov. 1998.

[20] M. Boutin, A. Benzakour, C. Despins, and S. Affes, "Characterization and modeling of a wireless channel at 2.4 and 5.8 GHz in underground tunnels," in *Proc. IEEE Wireless Commun. Syst. Symp. (ISWCS'06)*, pp. 517-521, Sep. 2006.

[21] J. M. Molina-Garcia-Pardo, M. Lienard, P. Degauque, D. G. Dudley, and L. Juan-Llacer, "Interpretation of MIMO channel characteristics in rectangular tunnels from modal theory," *IEEE Trans. Veh. Technol.*, vol. 57, no. 3, pp. 1974-1979, May 2008.

[22] M. Lienard and P. Degauque, "Mobile telecommunication in mine: characterization of the radio channel," in *Proc. IEEE Electrotechnical Conf. (MELECON apos'96)*, vol. 3, pp. 1663-1665, May 1996.

[23] H. Y. Yee, L. B. Felsen, and J. B. Keller, "Ray theory of reflection from the open end of a waveguide," *SIAM J. Appl. Math.*, vol. 16, no.2, pp. 268-300, Mar. 1968.

[24] P. Deift and X. Zhou, "A steepest descent method for oscillatory Riemann-Hilbert problems: asymptotics for the MKdV equation," *Ann. Math.*, vol. 137, no.2, pp. 295-368, 1993.

[25] G. L. Stuber, *Principles of Mobile Communication*. Boston : Kluwer Academic, 2001.

[26] R. E. Collin, *Field Theory of Guided Waves*. New York: IEEE Press, 1991.

[27] D. R. Frankl, *Electromagnetic Theory*. Englewwod Cliffs, NJ: Prentice-Hall, 1986.

Zhi Sun (S'06) received B.S. degree from Department of Communication Engineering, Beijing University of Posts and Telecommunications (BUPT), and M.S. degree from Department of Electronical Engineering Tsinghua University, Beijing, China in 2004 and 2007, respectively. Currently, he is a graduate research assistant in Broadband Wireless Networking Laboratory (BWN Lab), School of Electrical and Computer Engineering, Georgia Institute of Technology, Atlanta, GA. He is pursuing Ph.D. degree under the supervision of Prof. Ian F. Akyildiz. His current research interests are in Wireless Underground Communication Networks and Wireless Sensor Networks.

Ian F. Akyildiz (M'86-SM'89-F'96) received the B.S., M.S., and Ph.D. degrees in Computer Engineering from the University of Erlangen-Nurnberg, Germany, in 1978, 1981 and 1984, respectively. Currently, he is the Ken Byers Distinguished Chair Professor with the School of Electrical and Computer Engineering, Georgia Institute of Technology, Atlanta, the Director of Broadband Wireless Networking Laboratory and Chair of the Telecommunication Group at Georgia Tech. In June 2008, Dr. Akyildiz became an honorary professor with the School of Electrical Engineering at Universitat Politecnica de Catalunya (UPC) in Barcelona, Spain. He is also the Director of the newly founded N3Cat (NaNoNetworking Center in Catalunya). He is the Editor-in-Chief of COMPUTER NETWORKS (ELSEVIER) JOURNAL, and the founding Editor-in-Chief of the AD HOC NETWORKS (ELSEVIER) JOURNAL and the PHYSICAL COMMUNICATION (ELSEVIER) JOURNAL. His current research interests are in nano-networks, cognitive radio networks and wireless sensor networks.

He received the "Don Federico Santa Maria Medal" for his services to the Universidad of Federico Santa Maria, in 1986. From 1989 to 1998, he served as a National Lecturer for ACM and received the ACM Outstanding Distinguished Lecturer Award in 1994. He received the 1997 IEEE Leonard G. Abraham Prize Award (IEEE Communications Society) for his paper entitled "Multimedia Group Synchronization Protocols for Integrated Services Architectures" published in the IEEE JOURNAL ON SELECTED AREAS IN COMMUNICATIONS (JSAC) in January 1996. He received the 2002 IEEE Harry M. Goode Memorial Award (IEEE Computer Society) with the citation "for significant and pioneering contributions to advanced architectures and protocols for wireless and satellite networking." He received the 2003 IEEE Best Tutorial Award (IEEE Communication Society) for his paper entitled "A Survey on Sensor Networks," published in IEEE COMMUNICATIONS MAGAZINE, in August 2002. He also received the 2003 ACM Sigmobile Outstanding Contribution Award with the citation "for pioneering contributions in the area of mobility and resource management for wireless communication networks." He received the 2004 Georgia Tech Faculty Research Author Award for his "outstanding record of publications of papers between 1999 and 2003." He also received the 2005 Distinguished Faculty Achievement Award from School of ECE, Georgia Tech. He has been a Fellow of the Association for Computing Machinery (ACM) since 1996.